Hydrological-driven landslide in northwestern China measured by InSAR time series analysis

Qianyou Fan[1], Shuangcheng Zhang[1], Yufen Niu[2]

[1] College of Geology Engineering and Geomatics, Chang'an University, Xi'an 710054, China, (1980456976@qq.com; shuangcheng369@chd.edu.cn)
[2] College of Mining and Geomatics Engineering, Hebei University of Engineering, Handan 056038, China, (niuyufenpippa@163.com)

Key words: *time-series InSAR; landslide; precipitation*; *slope stability analysis*; *two-dimensional deformation*

ABSTRACT

The Lashagou landslide group is located in the transition zone between the Tibetan Plateau and Loess Plateau and is a typical shallow loess landslide group. Precipitation is a major hydrologic trigger for landslides in the northwestern China. Monitoring landslide movement constitutes a critical and requisite component of landslide hazard mitigation. Multi-track InSAR time series analysis can extract the 3D displacement of landslide, provide an indication of landslide occurrence and extent. In addition, quantifying the interaction between precipitation and landslide initiation and mobility to empirically determine the precipitation threshold associated with landslide movement is crucial for mitigating landslide hazards. In this paper, we highlight the results on mapping landslides over the state of Lashagou landslide group. The deformation rate and time series deformation of the Lashagou landslide group in the line-of-sight (LOS) direction from February 2020 to February 2021 were calculated using ascending and descending Sentinel-1A and Stanford Method for Persistent Scatterers (StaMPS) techniques. Besides, we obtained the two-dimensional deformation of the Lashagou landslide group by combining the slip geometr, LOS deformation, and SAR satellite imaging geometry. The results show that Lashagou landslide group is in the creep deformation stage. We compared the time series deformation of the extracted InSAR with that of the projected GNSS, and find that the measured values of InSAR and GNSS are highly similar in amplitude and deformation trend. In addition, the safety operation of G310 highway under the Lashagou landslide group was evaluated according to the observed deformation. We conclude that concentrated continuous rainfall is the main driver of landslide displacement, and that satellite observations of landslide movement and analysis of hydrological variables have improved our understanding of landslide mechanisms.

I. INTRODUCTION

Landslide is a natural disaster caused by the shearing movement of the slope under the action of gravity, earthquake and rainfall (Strozzi *et al*., 2018). It plays an important role in the process of mountain evolution (Shi *et al*., 2021), and rainfall is one of the most important factors that induce the occurrence and development of landslides (Lu and Kim, 2021). Under the influence of heavy rainfall, surface water infiltration and groundwater runoff cause the groundwater inside the landslide to rise. This increases the pore water pressure, resulting in a significant reduction in soil strength, which is prone to landslide disaster (Zhang *et al*., 2014). It is important to note that rainfall-induced landslides tend to have a regional cluster effect, which can cause massive damage in a short period of time (Liu *et al*., 2016). For example, on September 16, 2011, 1162 shallow soil landslides were triggered by heavy rain in Nanjiang County, China (Zhang *et al*., 2016). The number of rainfall-induced landslides is expected to increase due to the frequent occurrence of extreme rainfall events caused by global climate change (Segoni *et al*., 2021). Therefore, early identification and longterm monitoring of rainfall-induced landslides are necessary to mitigate the damage caused by landslides.

Monitoring landslide movement helps people to understand the evolution of landslide morphological characteristics over time and the mechanism by which external forces (such as precipitation and groundwater level changes) control landslide movement (Hu *et al*., 2019). Moreover, the time series deformation can provide important information for the early warning of landslides (Intrieri *et al*., 2018), which plays an important role in the management of landslide disasters. Conventional slope monitoring methods can only obtain sparse measurements at a few locations on or within the affected slopes, such as from Global Navigation Satellite System (GNSS), inclinometers, crack gauges, and acoustic sensors (Shi *et al*., 2018; Song *et al*., 2021). To overcome this, numerous researchers have sought to utilise the spaceborne Interferometric Synthetic Aperture Radar (InSAR) measurement which can map an entire landslide body continuously at a high spatial resolution (Zhao *et al*., 2019) and enables the investigation of the spatiotemporal features of multisurface failures (Hu *et al*., 2020).

A major limitation of InSAR is that the resulting motion measurements are restricted to a one-dimensional line-of-sight (LOS) viewing geometry. However, surface motions generally occur in the three spatial dimensions (*i.e.*, east (E), north (N) and up (U)). This means that the InSAR analysis of a stack of synthetic aperture radar (SAR) images acquired in a single viewing geometry is not able to fully capture the magnitude and direction of surface motions (Fuhrmann and Garthwaite, 2019). As a consequence, these LOS measurements are hard to interpret and communicate to stakeholders unfamiliar with the concept of a 1D viewing geometry. Several methods have been proposed to solve this problem, but the weaknesses of each method cannot be neglected (Ao *et al.*, 2019).

The research object of this paper is the Lashagou landslide group. Based on the Sentinel-1A images of ascending and descending from February 2020 to February 2021, the millimeter-scale LOS deformation is extracted by StaMPS technique. Then, we obtained the 2D-deformation of the Lashagou landslide group by combining the slip geometry, LOS deformation, and SAR satellite imaging geometry. Meanwhile, according to the time series deformation, we found that there is a significant correlation between the accelerated deformation and rainfall of the Lashagou landslide group. Finally, the 2D-dimensional deformation helps us to clarify the magnitude and direction of the landslide deformation, which provides support for the dynamic analysis of the landslide.

II. Study Area

The study area is located in Linxia City, Gansu Province, which is the transition zone between the Tibetan Plateau and Loess Plateau. The geographical location is shown in Figures 1a and 1b. The geological structure of the study area, affected by the Himalayan orogeny, is a resurrection of old tectonic movement and large scale uneven lifting movement (Cai *et al.*, 2015). There are many valleys in the territory, with an average altitude of 2000 m. The landform types are low mountain valleys and piedmont hills, and the mountainous area accounts for 90% of the total area (Jia *et al.*, 2018).

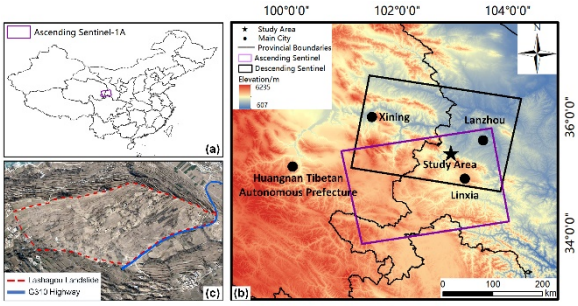

Figure 1. Overview of the study area: a) and b) The location of the study area and the coverage of satellite radar imagery; c) An optical image of the Lashagou landslide group.

The study area has a temperate continental climate, with a stable groundwater level of 11 m and an average annual rainfall of 350-500 mm. The rainfall from May to August accounts for 60%-78% of the annual average rainfall, and it mostly occurs in the form of heavy rain and extreme precipitation events (Wang *et al.*, 2020). Longterm rainfall increases the groundwater level, reduces the mechanical properties of the soil layer, which is prone to landslide disasters.

III. Data and Methods

A. *SAR Datasets*

The SAR images processed are Sentinel-1 Terrain Observation by Progressive Scans (TOPS) data in Interferometric Wide (IW) swath mode with a spatial resolution of about 2.3 m in range and 13.9 m in azimuth. The Sentinel satellite is a satellite constellation consisting of two satellites (Sentinel-1A/B) developed by the European Space Agency (ESA) for the Copernicus Global Observation Program. It uses C-band imaging with a wavelength of 5.6 cm. 29 Sentinel-1 images in the descending track and 32 images in the ascending track from 9 February 2020 to 27 February 2021 with a minimum temporal baseline of 12 days were collected.

According to the principle of maximum overall coherence, the GAMMA software was used to generate interferograms which started with the coregistration of Single Look Complex (SLC) images to a common primary image (31 August 2020 for ascending and 24 September 2020 for descending). The specific acquisition dates and spatiotemporal baseline combinations of the ascending and descending datasets are shown in Figure 2. In this paper, AW3D 30 DEM (ALOS World 3D Digital Surface Model) with a resolution of 30 m is used to eliminate the influence of terrain fluctuations, and high-precision DEM with a resolution of better than 0.2 m obtained by unmanned aerial vehicle (UAV) is used to calculate the slope angle and aspect of the Lashagou landslide group. In addition, this paper obtained the observation data of two GNSS stations (BZ01 and BZ02) located on the Lashagou landslide to verify the InSAR results, and obtained the daily rainfall data of the Linxia meteorological station from 2020 to 2021 for the analysis of factors affecting the landslide stability.

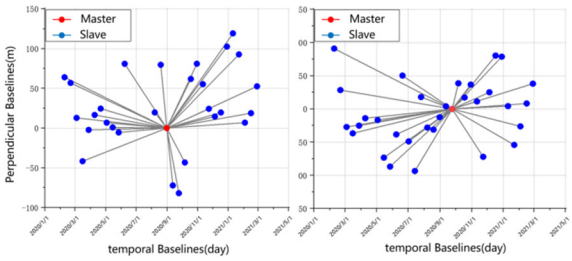

Figure 2. Temporal spatial baseline graph of (a) ascending and (b) descending Sentinel-1A Interferometric Pairs.

B. *StaMPS Processing*

A network of interferograms in single look can be generated and geocoded based on the resampled SLC images and a 30 m DEM after the coregistration. The tropospheric delay correction from Generic Atmospheric Correction Online Service (GACOS) for InSAR was then applied to these interferograms (Yu *et al*., 2017). The interferograms with tropospheric correction were imported into the StaMPS software (Hooper *et al*., 2012) to perform the PS analysis. Pixels with an amplitude dispersion index lower than 0.45 were selected as the "first-round" coherent pixels. The "second-round" coherent pixels were identified based on the characteristics of their phase noise.

After correcting the look-angle error and squint-angle error, the wrapped phase was unwrapped using a 3D-dimensional phase unwrapping method. Subsequently, spatial correlation errors were removed by high-pass filtering of the unwrapped data over time, followed by low-pass filtering in space. Finally, we obtained the LOS velocity and time series deformation using an SVD (Singular Value Decomposition) method.

C. *Method for 2D-dimensional Deformation*

In this paper, the sliding surface is used as the reference surface to observe the movement of the landslide. Under the action of natural forces, the sliding body has a larger terrain drop on the slope of the sliding surface, which is easy to generate a large gravitational potential energy and promote its own displacement. It can be seen that the changes of the slope and aspect of the sliding surface can reflect the overall movement intensity and direction of the landslide, which is just conforms to the law of the landslide movement. Therefore, this paper introduces two terrain factors, the slope and the aspect, to construct the sliding surface coordinates of the landslide movement. It is worth noting that the actual sliding surface of a landslide is often a changing surface. Since the specific shape of the sliding surface cannot be known, a uniform sliding surface is used in this paper to replace the actual sliding surface (Shi, *et al*., 2020).

Figure 3 shows the geometric relationship between the sliding surface coordinate system and the "North-East-Up" (NEU) coordinate system. d_T, d_V, and d_z represent the deformation vectors on the three axes of the sliding surface coordinate system. d_N, d_E, and d_U represent the deformation vectors on the three axes of the NEU coordinate system, and α and β represent the slope and aspect of the sliding surface, respectively. According to its geometric relationship, there are deformation projections of d_T and d_z in both the horizontal and vertical directions. Because the slope axis T and the normal axis Z are in the same vertical plane, the deformation projections of d_T and d_z on the horizontal plane should be overlapped, while d_V perpendicular to the vertical plane, the deformation projection in the vertical direction is zero. d_V is located in the horizontal plane, and there are deformation projections in the east-west and north-south directions. From this, the projection relationship matrix of the deformation between the sliding surface coordinate system and the NEU coordinate system can be obtained (Eq. 1):

$$\begin{bmatrix} d_E \\ d_N \\ d_U \end{bmatrix} = \begin{bmatrix} cos\alpha sin\beta & -cos\beta & sin\alpha sin\beta \\ cos\alpha cos\beta & sin\beta & sin\alpha cos\beta \\ -sin\alpha & 0 & cos\alpha \end{bmatrix} \begin{bmatrix} d_T \\ d_V \\ d_Z \end{bmatrix} \quad (1)$$

It is stipulated that the movement towards the satellite is positive, and the movement away from the satellite is negative.

According to the SAR satellite imaging geometry, the surface deformation in the LOS direction (d_{LOS}) is the sum of the projection of deformation in the east-west (d_E), north-south (d_N), and vertical (d_U) directions, as shown in Eq. (2):

$$d_{LOS} = [cos\theta \quad sin\theta sin\varphi \quad -sin\theta cos\varphi] \begin{bmatrix} d_U \\ d_N \\ d_E \end{bmatrix} \quad (2)$$

where θ is the incident angle of the radar satellite
φ is the heading angle of the radar satellite

In the natural environment, the sliding body usually moves downward along the sliding direction under the force of gravity. In the absence of strong external forces (such as artificial slope changes, etc.), the deformation along the normal direction of the sliding surface is much smaller than the deformation in other directions. Therefore, the deformation along the normal direction $d_z$is regarded as a zero constant in this paper. Combining Equations 1 and 2, the projection relationship matrix of the deformation on the sliding surface coordinate system and the LOS direction of the radar satellite can be obtained, as follows (Eq. 3):

$$\begin{bmatrix} d_T \\ d_V \end{bmatrix} = \begin{bmatrix} a_1 & b_1 \\ a_2 & b_2 \end{bmatrix}^{-1} \begin{bmatrix} d^a_{LOS} \\ d^d_{LOS} \end{bmatrix} \quad (3)$$

where $a_i = cos\theta_i * cos\alpha * cos\beta + sin\theta_i * sin\varphi_i * cos\alpha * cos\beta + sin\theta_i * cos\varphi_i * sin\alpha$

$b_i = cos\theta_i * sin\alpha * sin\beta + sin\theta_i * sin\varphi_i * sin\alpha * cos\beta - sin\theta_i * cos\varphi_i * cos\alpha$

IV. Results and Discussion

A. *InSAR Monitoring Results*

Using the ascending and descending SAR data, the velocity map in the LOS direction of the Lashagou landslide group between 9 February 2020 to 27 February 2021 was calculated. The results are shown in Figure 4, in which Figure 4a is the LOS velocity in the ascending direction, and Figure 4b is the LOS velocity in the descending direction. Note that negative values indicate that the landslide displacement is in the

direction away from the satellite, and positive values indicate that the landslide displacement is in the direction of the satellite. It can be seen from Figure 4 that the deformation of the Lashagou landslide group is mainly distributed in the northern part of Lashagou Village, where the deformation rate of the toe close to the road excavation is faster than that of the crown; thus, the entire landslide moves toward the G310 highway by pulling the crown from the toe. The maximum deformation in the LOS direction of the ascending and descending are -51 mm/yr and 49 mm/yr, respectively. The range and magnitude of the deformation regions calculated in different SAR datasets in the same time period are highly consistent. However, because different SAR satellites have different imaging geometries, and the displacement patterns at different locations of the same landslide may be different, resulting in different deformation features in the southern part of the study area.

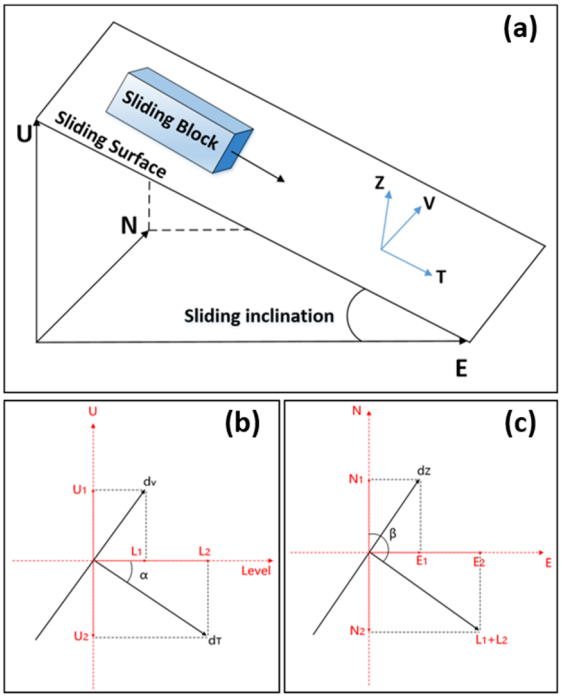

Figure 3. a) The coordinate system of the sliding surface of landslides. b) and c) The geometric relationship between the sliding surface and *NEU* coordinate system.

The time series deformation measurements of two GNSS stations (BZ01 and BZ02) located at the toe of the Lashagou landslide group were used to verify the accuracy of the InSAR measurements. Their specific locations are indicated by black triangles in Figure 4. In this study, the GNSS deformation observations in the three directions of the NEU are converted to the LOS direction of the radar according to Equation 2. Figure 5 shows the comparison results of the two GNSS stations and the observation values of the adjacent PS points. Figures 5a to 5b are the comparison of ascending InSAR and BZ01, ascending InSAR and BZ02, descending InSAR and BZ01, and descending InSAR and BZ02, respectively. Since the GNSS stations and PS points are not completely coincident, and there are certain errors in both monitoring techniques, the two measurements are not completely consistent. The MAE (Mean Absolute Error) and RMSE (Root Mean Square Error) are shown in Table 1. The maximum MAD and RMSE are 2.64 mm and 2.3 mm, respectively. However, such disparities are notably small in magnitude with respect to the deformation measurements. Therefore, we could conclude that the measurements derived by StaMPS are reliable.

Table 1. Comparison of InSAR and GNSS monitoring results

SAR dataset	GNSS station	Mean absolute error [mm]	Root mean square error [mm]
Ascending	BZ01	2.64	2.30
	BZ02	2.23	1.68
Descending	BZ01	2.51	1.95
	BZ02	2.35	2.00

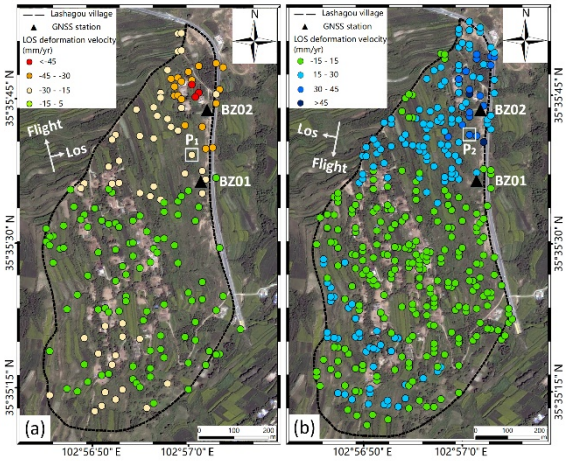

Figure 4. Surface average deformation rate maps in the LOS direction, (a) ascending and (b) descending.

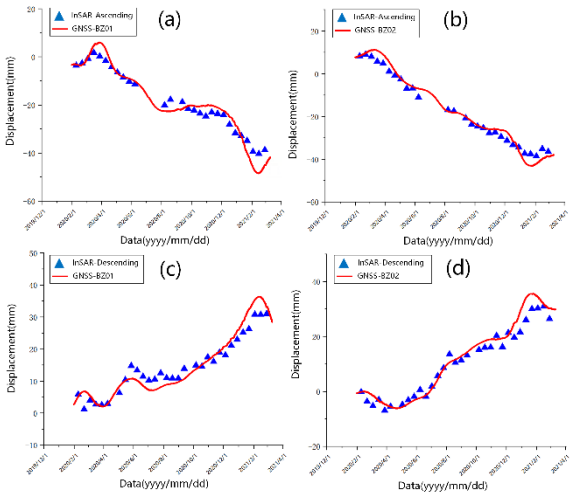

Figure 5. The comparison of LOS time series deformation between InSAR and GNSS.

B. *2D Displacement Results*

In this paper, the LOS velocity in the ascending and descending orbits is used to calculate the two-dimensional deformation velocity of the Lashagou landslide group on the sliding surface according to Equation 3, as shown in Figure 6. Figure 6a shows the deformation velocity along the sliding direction of the landslide on the sliding surface, Figure 6b shows the deformation velocity along the vertical direction on the sliding surface, and Figure 6c shows the two-dimensional deformation velocity on the sliding surface. The red arrows in the figure represent the displacement direction and magnitude of the landslide.

The two-dimensional deformation velocity on the sliding surface clearly shows the magnitude and direction of landslide deformation. Obviously, the deformation along the slope is significantly larger than that in the vertical direction. The maximum sliding deformation rate is 48 mm/yr, and the displacement directions are almost downwards along the slope. The deformation magnitude in the northern part of the landslide group is significantly larger than that in other areas (Figure 6a). The maximum vertical deformation velocity is 49 mm/yr, and the displacement direction varies greatly with the terrain. Obviously, there are two vertical deformation regions in the study area with opposite directions (Figure 6b). In the northern part of the study area, the landslide group moved in the direction of 30° east-north, and the deformation was relatively severe; on the contrary, in the northern part of the study area, the landslide group moved in the direction of 30° south-west, and the deformation was relatively stable. As Figure 6c shows, the maximum two-dimensional deformation of Lashagou landslide group is 68 mm/yr, and the deformation in the northern area is the most severe. The deformation range is consistent with the deformation characteristics reflected by the InSAR LOS measurements. Therefore, the northern region is the most unstable active block in the Lashagou landslide group, because of the favorable free-face conditions, higher sliding degrees of freedom, and larger sliding force caused by the steep terrain. It is prone to cause overall deformation and failure under the force of external factors, such as rainfall, which seriously threatens the safe operation and driving safety of the G310 highway. Therefore, it is necessary to monitor the deformation trend of the active deformed slope in real time.

C. *Discussion*

To analyze the control mechanism of rainfall and freeze-thaw cycles for the Lashagou landslide group, two PS pixels (P1 and P2) and two GNSS stations (BZ01 and BZ02) were selected for time series analysis. Figure 7a is the time series deformation of BZ01 and P2 obtained from the descending LOS deformation results, and Figure 7b is the time series deformation of BZ02 and P1 obtained from the ascending LOS deformation results. Figure 7c illustrates the changes of rainfall during the experiment and the solid blue line is the cumulative rainfall for 30 days. The gray columns indicate freezing periods corresponding to the period from mid-November of each year to mid-February of the following year, and the purple columns indicate freeze-thaw cycle periods corresponding to early November and late February to mid-March each year.

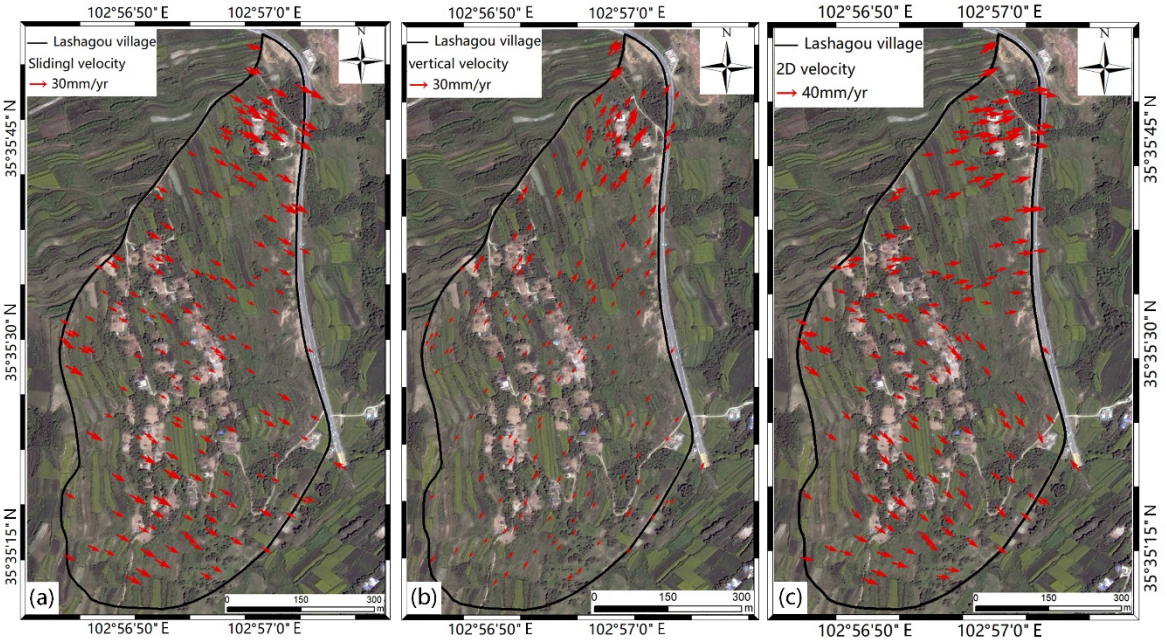

Figure 6. Two-dimensional deformation: a) Deformation along the sliding direction; b) Deformation along the vertical direction; c) Two-dimensional deformation on the sliding surface.

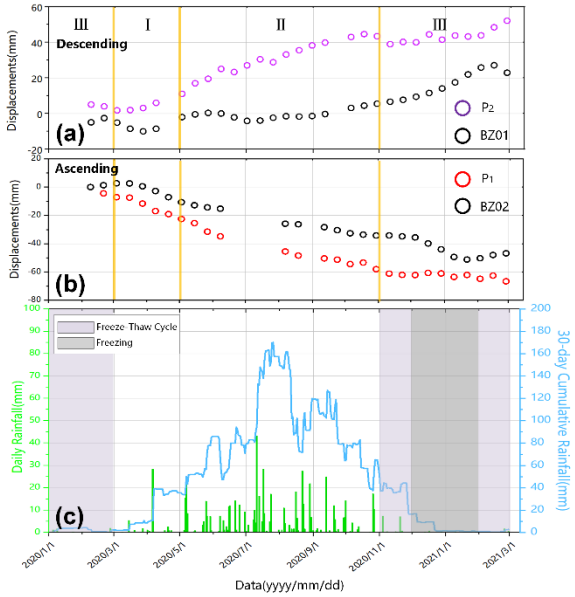

Figure 7. a) and b) Time series deformations of descending and ascending orbits, respectively. c) Relationships among landslide displacements and precipitation.

The landslide displacement is divided into three stages according to the changes of daily rainfall and 30 day cumulative rainfall. In the first stage (March to May), the temperature of the study area rose from about minus 20 ℃ to above zero, and the surface water changed from solid to liquid (Cai *et al*., 2015). The rapid snowmelt and surface water infiltration soften the soil near the permeable layer, reduce the shear strength significantly, and form a weak structural surface (Shi, *et al*., 2020). The release and flow of groundwater may cause different weak discontinuities to connect with each other and gradually penetrate, thus forming sliding zones. The landslide starts to slide along the sliding zone under the forces of gravity and other sliding forces. In the second stage (May to October), the precipitation is concentrated. At this time, rainfall infiltration or the rising groundwater level will lead to an increase in the gravitational potential energy of the landslide and a decrease in the frictional resistance of the sliding zone (Hu *et al*., 2020), which will cause the landslide to be in a state of continuous accelerated downhill movement in the rainy season. In the third stage (November to February of the following year), the temperature dropped sharply, and the average temperature was negative. During this period, the exposed sliding zone at the free surface of the landslide froze, which increased the shear strength and thus limited the shearing out of the landslide (Zhao *et al*., 2019). The downhill movement of the slope began to slow until it stabilized. Therefore, the groundwater level changes caused by rainfall and soil freeze-thaw cycles are the main reasons for the continuous deformation of the Lashagou landslide group.

V. Conclusions

In this paper, the two-dimensional deformation of the Lashagou landslide group are obtained by using the Sentinel-1A images and the StaMPS method assisted by GACOS. The time series analysis was carried out on the landslide hazard area and the influence of rainfall, human activities and other factors on the stability of the landslide was discussed. The results of the InSAR LOS measurements show that the deformation of the Lashagou landslide group is mainly distributed in the northern area. The deformation rate of the toe close to the road excavation is faster than that of the crown; thus, the entire landslide moves toward the G310 highway by pulling the crown from the toe. Through the comparative analysis with the daily rainfall data, it is found that the groundwater level change caused by rainfall and freeze-thaw cycle are the main reasons for the continuous deformation of the Lashagou landslide group.

The two-dimensional deformation of the sliding surface obtained from the LOS deformation shows that the deformation of the Lashagou landslide group along the sliding direction is generally greater than that of the vertical direction. The two-dimensional deformation of the study area is up to 68 mm/yr, and the persistent deformation in the northern area was caused by the human activities and slop excavation. Compared with the InSAR LOS measurements, the two-dimensional deformation clearly shows the deformation characterristics of the Lashagou landslide group, and the magnitude and direction of landslide deformation in different areas are clearly defined. This helps people better understand landslides and provides important and reliable deformation information for landslide management. This is helpful to improve our understanding of the spatiotemporal evolution of its morphological characteristics and the control mechanism of the influences of internal and external forces on landslide deformation.

VI. Acknowledgements

The authors are thankful for the free using of StaMPS. Sentinel-1 data were provided by ESA.

References

Ao, M., Zhang, L., Shi, X.G., Liao, M.S., and Dong, J. (2019). Measurement of the Three-Dimensional Surface Deformation of the Jiaju Landslide Using a Surface-Parallel Flow Model. *Remote Sensing Letters*, Vol. 10, No. 8, pp. 776-785.

Cai, G.Z., Yang, Z.H., Wang, D.P., Sun, Y.L., and Zhou, S.D. (2015). Cause Analysis and Defense Countermeasures of Geological Hazards in Linxia City, Gansu Province. *Journal of Agricultural Catastrophology*, Vol. 5, No. 4, pp. 32-35.

Fuhrmann, T., and Garthwaite, M.C. (2019). Resolving Three-Dimensional Surface Motion with InSAR: Constraints from Multi-Geometry Data Fusion. *Remote Sensing*, Vol. 11, No. 3, pp. 241-261.

Hu, X., Bürgmann, R., Lu, Z., Handwerger, A.L., Wang, T., and Miao, R.Z. (2019). Mobility, Thickness, and Hydraulic Diffusivity of the Slow-Moving Monroe Landslide in California Revealed by L-Band Satellite Radar Interferometry. *Journal of Geophysical Research: Solid Earth*, Vol. 124, No. 7, pp. 7504-7518.

Hu, X., Bürgmann, R., Schulz, W.H., and Fielding, E.J. (2020). Four-Dimensional Surface Motions of the Slumgullion Landslide and Quantification of Hydrometeorological Forcing. *Nature Communications*, Vol. 11, No. 1.

Hooper, A., Bekaert, D., Spaans, K., and Arıkan, M. (2012). Recent Advances InSAR Interferometry Time Series Analysis for Measuring Crustal Deformation. *Tectonophysics*, Vol. 514, pp. 1–13.

Intrieri, E., Raspini, F., Fumagalli, A., Lu, P., Del Conte, S., Farina, P., Allievi, J., Ferretti, A., and Casagli, N. (2018). The Maoxian Landslide as Seen from Space: Detecting Precursors of Failure with Sentinel-1 Data. *Landslides*.

Jia, C.P., Jin, Z.X., Yang, P., and Tang, Z.L. (2018). Stability Analysis on Landslide in Section K181 + 840 ~ K182 + 040 of Lin-Da Highway. J*ournal of Lanzhou Petrochemical Polytechnic*, Vol. 18, No. 3, pp. 26-28.

Liu, L., Yin, K.L., Wang, J.J., Zhang, J., and Huang, F.M. (2016). Dynamic Evaluation of Regional Landslide Hazard Due to Rainfall: A Case Study in Wanzhou Central District, Three Gorges Reservoir. *Chinese Journal of Rock Mechanics and Engineering*, Vol. 35, No. 3, pp. 558-569.

Lu, Z., and Kim, J. (2021). A Framework for Studying Hydrology-Driven Landslide Hazards in Northwestern US Using Satellite InSAR, Precipitation and Soil Moisture Observations: Early Results and Future Directions. *GeoHazards*, Vol. 2, pp. 17-40.

Segoni, S., Gariano, S.L., and Rosi, A. (2021). Preface to the Special Issue "Rainfall Thresholds and Other Approaches for Landslide Prediction and Early Warning". *Water*, Vol. 13, No. 3.

Shi, X.G., Zhang, L., Zhou C., Li, M.H., and Liao, M.S. (2018). Retrieval of Time Series Three-Dimensional Landslide Surface Displacements from Multi-Angular SAR Observations. *Landslides*.

Shi, G.L., Chen, Q., Liu, X.W., Yang, Y.H., Xu, Q., and Zhao, J.J. (2020). Deformation Velocity Field in the Aspect Direction of an Ancient Landslide in Taoping Village Derived from Ascending and Descending Sentinel-1a Data. *Journal of Engineering Geology*.

Shi, X.G., Hu, X., Sitar, N., Kayen, R., Qi, S.W., Jiang, H.G., Wang, X.D., and Zhang, L. (2021). Hydrological Control Shift from River Level to Rainfall in the Reactivated Guobu Slope Besides the Laxiwa Hydropower Station in China. *Remote Sensing of Environment*, Vol. 265.

Song, C., Yu, C., Li, Z.H., Pazzi, V., Del Soldato, M., Cruz, A., and Utili, S. (2021). Landslide Geometry and Activity in Villa De La Independencia (Bolivia) Revealed by InSAR and Seismic Noise Measurements. *Landslides*.

Strozzi, T., Klimeš, J., Frey, H., Huggel, C., Wegmüller, U., and Rapre, A.C. (2018). Satellite SAR Interferometry for the Improved Assessment of the State of Activity of Landslides: A Case Study from the Cordilleras of Peru. *Remote Sensing of Environment*, Vol. 217, pp. 111-125.

Wang, M.H., Zhao, H., Ni, T.X., Chen, L., and Wang, L.C. (2020). Stability Analysis of the Nalesi Ancient Landslide Based on the Discontinuous Layout Optimization. *Northwestern Geology*, Vol. 53, No. 1, pp. 234-242.

Yu, C., Li, Z.H., and Penna, N.T. (2017). Interferometric Synthetic Aperture Radar Atmospheric Correction Using a GNSS-Based Iterative Tropospheric Decomposition Model. *Remote Sensing of Environment*, Vol. 204, pp. 109-121.

Zhang, Q., Xu, Q., Yi, J.S., Xu, L., and Ma, Z.G. (2016). Rainfall Infiltration Depth and Formation Mechanism of Slow-Inclination Soil Landslides in Nanjiang. *Chinese Journal of Geotechnical Engineering*, Vol. 38, No. 8, pp. 1447-1455.

Zhang, S.R., Tan, Y.S., Wang, C., and Yu, M. (2014). Influence of Heavy Rainfall Characteristics on Saturated-Unsaturated Slope Failure. *Chinese Journal of Rock Mechanics and Engineering*, Vol. 33, No. 2, pp. 4102-4112.

Zhao, C.Y., Liu, X.J., Zhang, Q., Peng, J.B., and Xu, Q. (2019). Research on Loess Landslide Identification, Monitoring and Failure Mode with InSAR Technique in Heifangtai, Gansu. *Geomatics and Information Science of Wuhan University*, Vol. 44, No. 7, pp. 996-1007.